Journal of Photochemistry and Photobiology A: Chemistry 212 (2010) 8–13

Contents lists available at ScienceDirect

Journal of Photochemistry and Photobiology A: Chemistry

journal homepage: www.elsevier.com/locate/jphotochem

The hydrothermal synthesis of BiOBr flakes for visible-light-responsive photocatalytic degradation of methyl orange

Zheng Jiang[a,b,c,*], Fan Yang[b], Guidong Yang[a], Liang Kong[a], Martin O. Jones[a,d], Tiancun Xiao[a], Peter P. Edwards[a,**]

[a] Department of Chemistry, Inorganic Chemistry Laboratory, University of Oxford, OX1 3QR, UK
[b] State Key Laboratory of Multiple Phase Complex Systems, Institute of Process Engineering, Chinese Academy of Sciences, Beijing 100080, China
[c] Jesus College, University of Oxford, OX1 3DW, UK
[d] ISIS, Science and Technology Facilities Council, Rutherford Appleton Laboratory, Harwell Science and Innovation Campus, Didcot, OX11 0QX, UK

ARTICLE INFO

Article history:
Received 14 December 2009
Received in revised form 19 February 2010
Accepted 15 March 2010
Available online 21 March 2010

Keywords:
BiOBr
Flake
Hydrothermal synthesis
Visible light
Photocatalysis

ABSTRACT

Flake-like BiOBr semiconductors have been prepared using hydrothermal synthesis with meticulous control of synthesis parameters and used for photocatalytic degradation of methyl orange. XRD, SEM and UV–vis characterizations have been performed to study the obtained BiOBr materials. The results indicate that the morphology and crystallite size of BiOBr depend significantly on the temperature and duration of the hydrothermal syntheses. Diffuse UV–vis spectra show the BiOBr materials to be indirect semiconductors with an optical bandgap of approximately 2.92 eV, which is essentially unaffected by the synthesis parameters. The hydrothermal-synthesized BiOBr flakes exhibit noticeable activity for photodegradation of methyl orange under visible light (>400 nm) illumination, with the BiOBr synthesized by hydrothermal treatment at 120 °C for 6 h exhibiting superior photocatalytic performance in these flakes. The excellent activity and photo-stability reveal that BiOBr is a promising visible-light-responsive photocatalyst.

1. Introduction

Heterogeneous photocatalysis for the environment remediation and solar energy conversion has aroused extensive interest in the past decade [1–3]. For the practical application of photocatalysis, an environmentally robust and inexpensive photocatalyst is a crucial component [4]. Among the diverse photocatalytic materials, nano-scaled TiO_2 is mostly studied, however, it can only be activated by irradiation under UV, which comprises less than 5% of the solar spectrum [5–7]. In order to utilise the visible light (accounting for 43% energy in solar spectrum) and harvest solar energy efficiently, intensive efforts have been made to develop visible-light-responsive photocatalysts, such as metal/nonmetal doped TiO_2 [7–12], inorganic bismuth compounds (Bi_2WO_6 [13], Bi_2MoO_6 [14] and $BiVO_4$ [15,16]) and ferrites [17], *etc.* Although most of the photocatalysts show markedly visible-light-responsive activity, their stabilities, the relationship between structure and photocatalytic reactivity and the photocatalysis mechanisms remain uncertain [9,10,13–18]. Therefore, synthesizing novel visible-light responsive photocatalysts and exploring their photocatalysis performance are of great interest and potential reward [19].

Bismuth oxyhalide compounds have recently been found to be potential photocatalysts under UV or visible-light illumination [19–24]. Among the bismuth oxyhalides, BiOBr is of particular importance because it is visible-light responsive, relatively stable under light irradiation and superior to the commercialized Degussa P25 (TiO_2 aerosol mixture comprising of Rutile and anatase phases) under UV illumination [25–27]. BiOBr is a layer-structured semiconductor that consists of tetragonal $[Bi_2O_2]$ positive slabs, which are interleaved by double slabs of bromide to form $[Bi_2O_2Br_2]$ layers along the *c* axis. This intrinsic lamellar structure endows BiOBr with unique electrical, optical and catalytic activity [24,25]. Besides the intrinsic crystal structure, the photocatalytic performance of a specific semiconductor is closely related to its particle size and crystallinity, while these parameters significantly depend on the synthesis routes [7,8,25–28]. The various synthesis methods of BiOBr also exert different effects on its particle size and morphology and, as a consequence, a remarkable effect on photocatalytic activity [25–28]. Therefore, it is a necessity to discover a general suitable synthesis method that enables the fundamental understanding of the crystalline structure evolution and its influence on photocatalytic performance of BiOBr.

* Corresponding author at: Department of Chemistry, Inorganic Chemistry Laboratory, University of Oxford, South Parks Road, Oxford OX1 3QR, UK. Tel.: +44 1865 272660.
** Corresponding author. Tel.: +44 1865 272646; fax: +44 1865 272656.
E-mail addresses: zhjiang76@hotmail.com (Z. Jiang), peter.edwards@chem.ox.ac.uk (P.P. Edwards).

1010-6030/$ – see front matter © 2010 Elsevier B.V. All rights reserved.
doi:10.1016/j.jphotochem.2010.03.004

BiOBr can be simply prepared through a hydrolysis method, however, the resulting product is poorly crystalline and the synthesis process is uncontrollable [24]. Reverse micro-emulsion synthesis has been adopted to prepare nanosized BiOBr, but the synthesis process is very complicated, time-consuming, costly and not guaranteed to produce crystalline phases [28]. While solvothermal synthesis has been reported as a good strategy to prepare assembled BiOBr nano-crystal, the organic solvent involved is environmentally harmful [26]. In contrast, hydrothermal synthesis is a potentially environment-friendly and cost-effective synthesis methodology for a variety of nano-materials [29,30]. Due to its versatility and ability to control particle size, shape and crystallinity by adjusting the hydrothermal treatment parameters, hydrothermal synthesis has been used to prepare bismuth oxyhalides in alkaline aqueous solutions at high temperature [31,32]. However, the basic environment of the alkaline aqueous solutions leads to varied composition and morphology of bismuth oxyhalides at elevated synthesis temperatures [31,32]. So far, there is neither report concerning hydrothermal growth of BiOBr in acidic conditions nor the effect of the synthesis parameters on its morphology, structure and photocatalysis properties under visible-light illumination.

In this study, we have successfully prepared a number of pure BiOBr samples by controlling the hydrothermal synthesis parameters. The morphologies, particle and crystallite sizes and photocatalytic activity are then characterized and correlated with the synthesis conditions. The stability of the sample from the optimized hydrothermal synthesis has also been explored. The visible-light responsive mechanism on BiOBr has been attentively discussed.

2. Experiment

2.1. Preparations of BiOBr

BiOBr samples were synthesized using a hydrothermal synthesis process with different treatment durations and temperatures. Typically, 0.97 g $Bi(NO_3)_3{\cdot}5H_2O$ was dissolved in 3 ml acetic acid (HAc), and the resulting solution was added to 30 ml de-ionized water containing 0.24 g KBr under vigorous stirring. Upon the adding of $Bi(NO_3)_3$/HAc solution, yellow precipitates were immediately observed which then became light yellow as addition was completed. After stirring for 20 min at room temperature, the suspension was transferred into a Teflon-lined stainless steel autoclave (40 ml capacity) and heated at the designated heating temperature and for the designated time. The resulting precipitate was filtrated, washed thoroughly with distilled water to remove any possible ionic species in the product, and then dried at 60 °C overnight. To reveal the effects of key synthesis parameters, such as hydrothermal treatment time and temperature, samples were synthesized at 120 °C for durations of 2, 6, 16 and 24 h, as well as at 150 and 180 °C, both under optimized time span (6 h as disclosed in the text).

2.2. Characterization

X-ray powder diffraction data of the prepared samples were recorded on a PANalytical X'Pert PRO at 40 kV, 30 mA. FE-SEM images were obtained on a JSM-6700F field emission scanning electron microscope operated at 10.0 kV. The compositions of the samples were tested by EDAX instrument equipped to JSM-6700F microscope. The UV–vis absorption spectra were measured by a HITACHI U-3310 spectrophotometer with scan rate of 300 nm/s.

2.3. Photocatalytic reaction

The catalytic degradation of 10 mg/L methyl orange (MO) aqueous solution was carried out to screen the photocatalysts and determine the optimum synthesis parameters. The photocatalytic reactor consists of an overhead 300 W Xenon lamp (PLS-SXE300, Beijing TrustTech) equipped with a UV filter (UVCUT400, Beijing TrustTech), which prevents transmission of light with wavelength lower than 400 nm and allows transmission of 400–780 nm visible light. Reaction suspensions were prepared by adding 0.1 g of BiOBr powder to 50 ml of MO in aqueous solution. Prior to light irradiation, the suspensions were sonocated in the dark for 30 min to establish absorption–desorption equilibrium of the dye on the catalyst surface. During the illumination, approximately 2 ml of suspension was removed from the reaction suspension by a micro-filter syringe and analyzed by the HITACHI U-3010 spectrophotometer. After each photo-activity test, both of the separated solid and solution were returned into the reaction system. The characteristic absorption peak of MO at 462 nm was used to determine the extent of MO degradation. The MO photo-degradation over P25 TiO_2 has been done under the same reaction conditions. Photocatalysis over the optimum BiOBr material has been undertaken on 15 separate occasions to investigate its stability.

3. Results and discussion

3.1. Characterizations of as-prepared powders

3.1.1. XRD analysis

The X-ray diffraction data of BiOBr samples prepared with different hydrothermal parameters are shown in Fig. 1(a) and (b). All the BiOBr samples synthesized using the hydrothermal method described earlier at different temperatures and durations are pure tetragonal phase BiOBr (JCPDS 73-2061) with well resolved (0 0 1), (0 1 1), (0 1 2), (1 1 0), (2 1 2) reflections [24]. As shown in Fig. 1(a), the prolongation of hydrothermal treatment leads to the intensity of the Bragg peaks of BiOBr getting higher and narrower, which is attributed to an increase of average particle from the 2 h synthesis to the 24 h synthesis. Indeed, the profile fitting analyses of the X-ray data sets for 2, 6, 16 and 24 h show average particle sizes of 84, 82, 85 and 93 nm, respectively. Fig. 1(b) shows X-ray diffraction data for BiOBr samples prepared at 120, 150 and 180 °C for 6 h, respectively. Here, increasing the temperature of hydrothermal treatment results in preferred oriental growth along the [0 0 1] direction. Clearly, the crystallite size and growth direction of the BiOBr samples strongly depends on both the synthesis temperature and the duration, with prolongation of hydrothermal treatment time leading to larger crystallite size and elevation of hydrothermal temperatures leading to anisotropic growth of BiOBr along the (0 0 1) crystal face. In addition, from the XRD and EDAX analyses (not shown), there are no observed stoichiometry changes regardless of the variation of the synthesis parameters (temperature and duration), suggesting that the components of the BiOBr samples are similar under the acidic synthesis conditions. However, alkaline hydrothermal syntheses at high temperature usually result in the formation of bismuth oxybromides of varied morphologies and compositions, such as plates and nanobelts [31]. The XRD results here reveal that acidic hydrothermal synthesis is a good methodology to prepare BiOBr crystalline flakes and study the structure evolution of bismuth oxyhalides.

3.1.2. SEM analysis

To obtain a better understanding of the morphology evolution of BiOBr materials, samples synthesized with varying hydrothermal duration at 120 °C were characterized by scanning electron microscopy (SEM). The corresponding SEM images are shown in Fig. 2. For hydrothermal synthesis at 120 °C/2 h, the obtained samples are flakes with average diameter approximately 600 nm and a thickness below 50 nm (Fig. 2(a)). The flakes then gradually grow larger and thicker as the hydrothermal synthesis duration increases

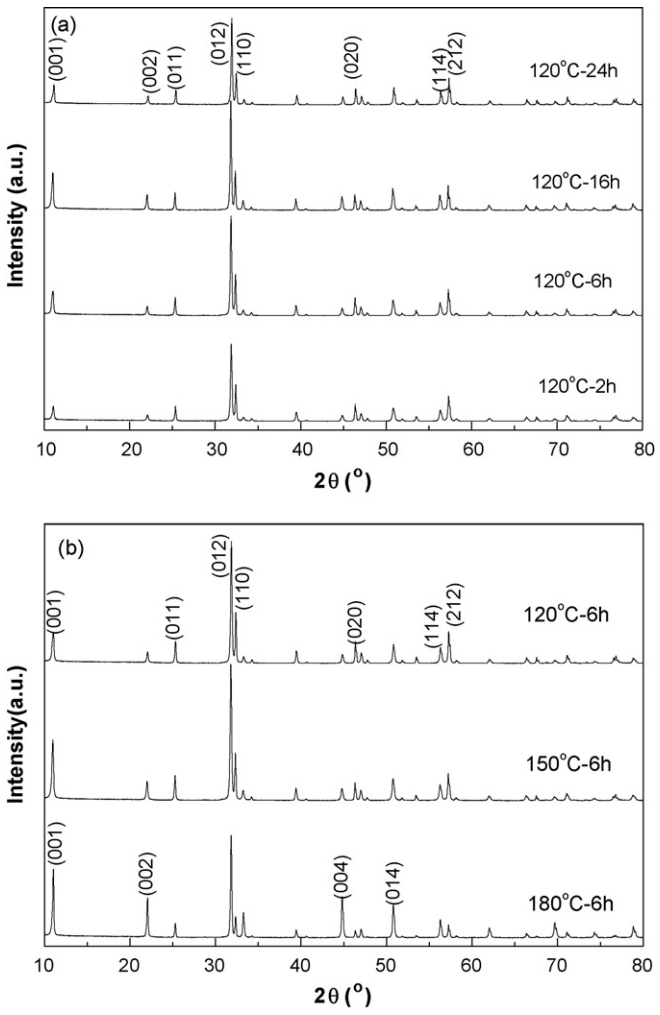

Fig. 1. X-ray diffraction data for BiOBr samples synthesized for 2–24 h at 120 °C (a) and BiOBr powders prepared at 120, 150 and 180 °C for 6 h.

(shown in Fig. 2(b)–(d)). After 24 h hydrothermal reaction, the diameter and thickness of BiOBr flake are observed to be up to 2 μm and 100 nm, respectively. These SEM images clearly show the sample synthesized for 24 h to have a more even distribution of larger particle sizes than is seen for lower synthesis times. This observation is consistent with the increase in average particle size observed by X-ray diffraction.

BiOBr samples synthesized at different temperatures for 6 h were also examined by SEM, and the results are shown in Fig. 3. Obviously, as the hydrothermal temperature increase, the diameter of BiOBr flakes synthesized at 180 °C is up to 6 μm, 10 times that of BiOBr synthesized at 120 °C, but the thickness of the samples grow slower, which is nearly the same with those of samples synthesized at 120 °C. These observations are consistent with the results obtained by X-ray diffraction, further evidencing the preferentially oriental growth along the (0 0 1) crystal direction and the benefits of acidic hydrothermal synthesis.

3.1.3. UV–vis diffuse reflectance spectroscopy

Fig. 4(a) shows the UV–vis diffuse reflectance spectra (DRS) of the BiOBr samples prepared at 120 °C for 2, 6, 16 and 24 h. The absorption edges of the BiOBr flakes locate in the range of 430–440 nm, corresponding to a band-gap energy (Eg) of approximately 2.85–2.92 eV. The Eg values are well consistent with the experimental value of sample prepared using co-precipitation method. Taking the sample prepared at 120 °C and 6 h as an example, we analyzed the shape of the reflectance spectra to estimate the transition characteristics (direct or indirect) of the sharp absorption edge. For semiconductors, the square of absorption coefficient is linear with respect to energy for direct optical transitions in the absorption edge region, whereas the square root of absorption coefficient is linear with energy for indirect transitions [19]. The plots of absorption squared (abs^2) versus energy and the square root of absorption ($abs^{1/2}$) versus energy for the BiOBr absorption edge region are presented in Fig. 4(b). The $abs^{1/2}$ versus energy plot is nearly linear, while the abs^2 versus energy deviates from the fitted straight line, which suggest that the absorption edge of BiOBr is caused by indirect transitions, namely, the

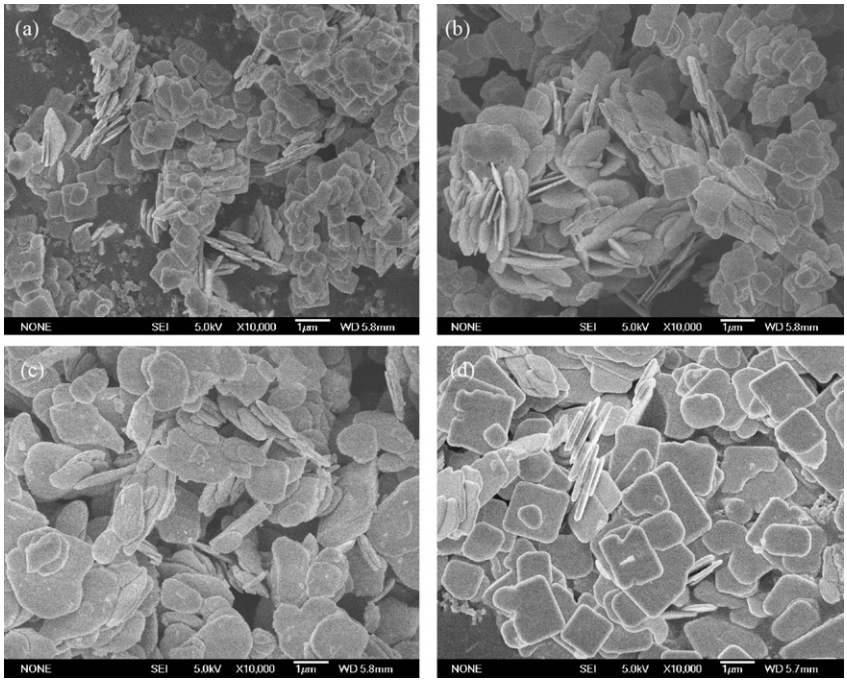

Fig. 2. The FE-SEM images of BiOBr samples treated at 120 °C with different hydrothermal reaction durations: (a) 2 h, (b) 6 h, (c) 16 h and (d) 24 h.

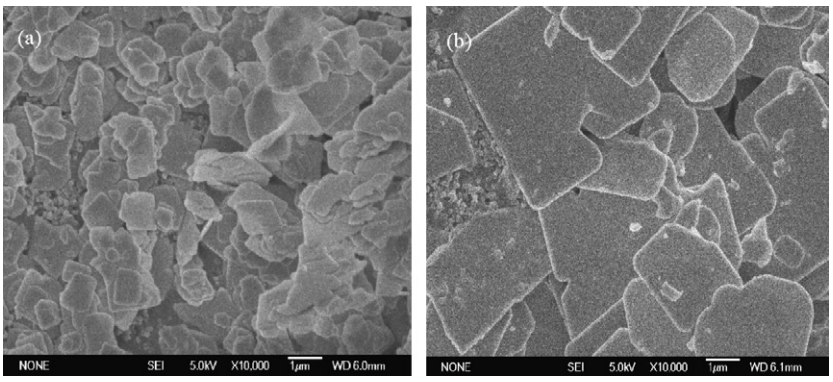

Fig. 3. The FE-SEM images of BiOBr samples treated for 6 h at: (a) 150 °C and (b) 180 °C.

BiOBr is an indirect semiconductor [19]. The samples prepared in the present hydrothermal synthesis method show similar diffuse reflection behaviour and no remarkable red-shift or blue-shift can be observed, which suggest that there is no significant quantum effect exhibited by the samples. This is reasonable because of the relatively large particle sizes of the samples compared to quantum dots, which are usually of the order of a few nanometers in size.

3.2. Photocatalytic activity

The influences of the hydrothermal synthesis parameters on the photocatalytic performance of MO decompositions over the as-prepared BiOBr flakes under visible-light irradiation are shown in Fig. 5(a) and (b). The BiOBr materials can be well dispersed under magnetic stirring, which promise the good transportation of MO in the solution to the BiOBr samples in photocatalysis tests. In order to exclude the dye-sensitizing effect over the photocatalysts, control experiments under the same conditions, where MO decomposes in the absence of photocatalyst and presence of P25 TiO_2 were studied as references. Fig. 5(a) shows the photocatalytic activity of BiOBr synthesized at 120 °C for 2, 6, 16, 24 h and control exper-

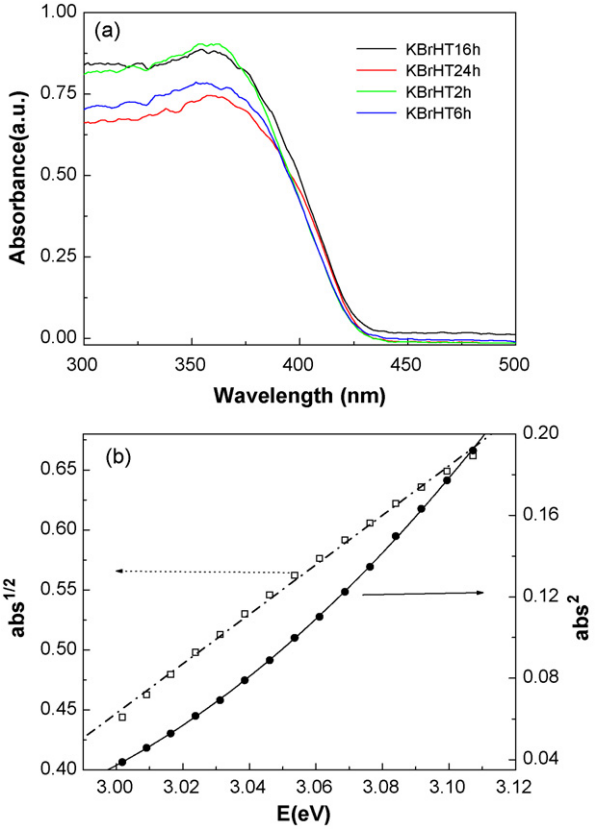

Fig. 4. The absorption spectra of BiOBr samples prepared at 120 °C for 2, 6, 16 and 24 h (a) and the plots of a absorption squared (abs^2) versus energy (open circles for experimental data and the dashed line for a linear fitting) and the square root of absorption ($abs^{1/2}$) versus energy for the BiOBr absorption (filled circles and solid line for polynomial fitting) in the absorption edge region of BiOBr samples prepared at 120 °C for 2, 6, 16 and 24 h.

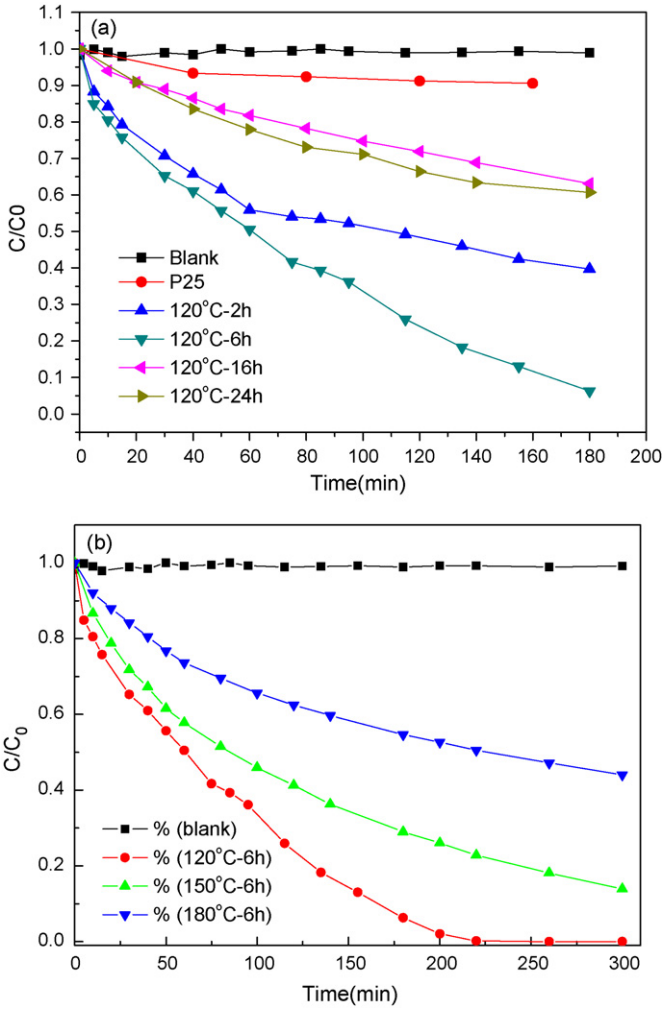

Fig. 5. MO decomposition over BiOBr samples prepared at 120 °C for 2, 6, 16 and 24 h (a) and BiOBr samples prepared at 120, 150 and 180 °C for 6 h under 300 W Xenon lamp irradiation (b) (C_0, initial concentration of MO; C, residual concentration of MO).

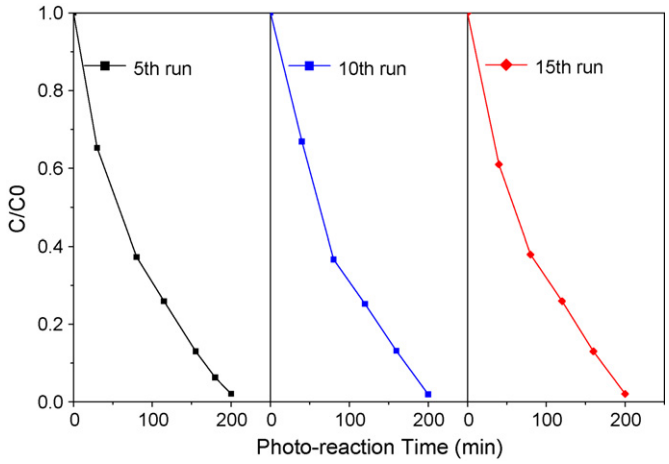

Fig. 6. Lifetime of visible-light photo-degradation MO over BiOBr synthesized with hydrothermal treatment at 120 °C/6 h (C_0, C: initial and residual concentration of MO, 300 W Xenon lamp irradiation).

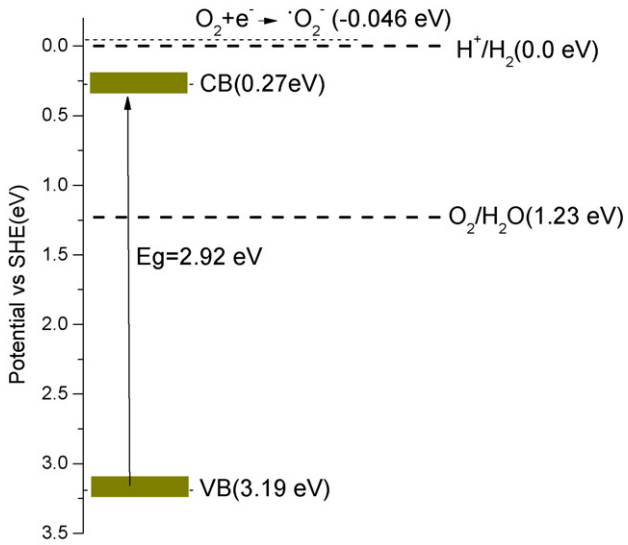

Fig. 7. Schematic band structure of BiOBr.

iments. There is a slight degradation of MO over P25 in the given reaction period (~3 h) due to the dye-sensitive visible-light photocatalytic effect on the surface of P25 [33], no degradation of MO in the absence of photocatalyst can be observed at all. In contrast, significant degradation has been observed on the as-prepared BiOBr photocatalysts. Here, the BiOBr synthesized with 6 h hydrothermal treatment shows best photo-degradation activity to MO, on which the 3 h MO decomposition extent is nearly twice and three times of those prepared with 2, 16 and 24 h treatments. The photocatalytic MO degradation performance on BiOBr samples synthesized for 16 and 24 h are almost identical, but far lower than those where synthesis was limited to 2 and 6 h. The effect of hydrothermal temperature on photocatalytic activity for the same reaction time is shown in Fig. 5(b). It can be seen that the MO photo-degradation activities on BiOBr photocatalysts decrease with the increase of hydrothermal reaction temperature between 120 and 180 °C, with BiOBr synthesized at 120 and 180 °C exhibiting the best and worst photocatalytic activities, respectively. Elevated hydrothermal temperature and prolonged hydrothermal duration promote crystallite growth but deteriorate its photocatalytic performance because of the increased particle sizes. In our cases, the optimum hydrothermal synthesis parameters for robust BiOBr are heating at 120 °C for about 6 h.

The lifetime of photocatalyst is important for practical applications. The photo-degradation of MO over the optimum BiOBr synthesized at 120 °C/6 h has been repeated 15 times under the same reaction conditions, by repeating the centrifugation of the BiOBr sample after completing the photocatalysis reaction and re-dispersing into 50 mL MO solution in each run. In the lifetime test (shown in Fig. 6), the selected BiOBr flakes exhibit nearly similar photocatalysis performance. The good photocatalytic stability proves that BiOBr is stable or just etched to a negligible degree.

3.3. *Visible-light-induced degradation mechanism*

The conductance and valence band (CB and VB) edge electrochemical potentials of BiOBr semiconductor are important factors to understand the photo-degradation mechanism of contaminants over BiOBr. The flat-band potential of BiOBr was calculated using an atom's Mulliken electronegativity theory: $E_{VB} = X_{BiOBr} - E^e + (1/2)Eg$ [34,35], where E_{VB} is the potential of valance band top, X_{BiOBr} is the electronegativity of the BiOBr, which is the geometric mean of the electronegativity of the constituent atoms, E^e is the energy of free electrons on the hydrogen scale (ca. 4.5 eV) and Eg is the band-gap energy of the BiOBr (2.92 eV). Fig. 7 shows a schematic band structure of BiOBr semiconductor based on the earlier calculation. It is theoretically speculated that the band edge potentials of CB and VB of BiOBr semiconductor are 0.27 and 3.19 eV with respect to the vacuum level, respectively. It can be seen that the calculated VB edge potential of BiOBr is more positive than the standard redox potentials of •OH/OH^- (1.99 eV), H_2O_2 (1.77 eV) and O_3 (2.07 eV) , suggesting that the photo-generated hole is far more oxidative than •OH radical, H_2O_2 and O_3. Moreover, the photo-generated holes could not oxidized OH^- to form the •OH radicals because of the more negative reduction potential of Bi^V/Bi^{III} [36]. Therefore, it is theoretically reasonable that the photo-degradation of MO could be attributed to the reaction with the photo-generated holes directly rather than the species such as •OH radicals, H_2O_2 and O_3 generated during the photocatalysis. The CB edge potential of BiOBr (0.27 eV) is not negative enough to reduce the O_2 molecule to the oxygen radical by the photo-excited electron, because the electrochemical potential for single-electron reduction of oxygen is −0.046 eV [37]. However, this cannot exclude the formation of oxygen radicals by photo-generated electrons from the higher conduction bands. The experimental evidence to evaluate or exclude the effects of the mentioned "intermediates" need to include hole scavengers with different redox potentials, and this work is ongoing.

4. Conclusion

Tetragonal phase BiOBr flakes have been prepared using an acidic hydrothermal synthesis with meticulous control of the synthesis parameters. The obtained BiOBr flakes are indirect transition semiconductors with intrinsic optical bandgaps of approximately 2.85–2.92 eV depending on the synthesis conditions. Controlling the synthesis condition, such as hydrothermal treatment temperature and time, allows us to tailor the diameters and thickness of BiOBr flakes produced. These BiOBr flakes are active for photo-degradation of methyl orange (MO) dye under visible-light irradiation. The optimum hydrothermal synthesis parameters for robust BiOBr photocatalyst are found to be hydrothermal treatment at 120 °C for 6 h. This photocatalyst exhibits excellent stability in 15 runs of visible-light-driven photo-degradation of MO under the same reaction conditions. The visible-light response of these BiOBr

samples has been reasonably attributed to the strong oxidation power of the photo-generated holes.

Acknowledgements

This work was financially supported by Oxford Challenge Seed Fund, UK Photocatalysis Network, UKSHEC (EPRSC). Dr Jiang acknowledges the Initiating Fund of President Award in Chinese Academy of Sciences, and the John Houghton Fellowship at Jesus College, Oxford University. We thank Dr. Patrick Dunlop from the Nanotechnology and Integrated Bioengineering Centre (NIBEC) in the University of Ulster, North Ireland, for his helps with UV–vis DRS. We acknowledge Mrs Linda Webb for her kind help with the manuscript revision.

References

[1] M.D. Hernandez-Alonso, F. Fresno, S. Suarez, J.M. Coronado, Energy Environ. Sci. 2 (2009) 1231–1257.
[2] S. Malato, P. Fernández-Ibáñez, M.I. Maldonado, J. Blanco, W. Gernjak, Catal. Today 147 (2009) 1–59.
[3] A. Fujishima, X. Zhang, D.A. Tryk, Surf. Sci. Rep. 63 (2008) 515–582.
[4] A. Mills, S. Le Hunte, J. Photochem. Photobiol. A 108 (1997) 1–35.
[5] A. Henglein, Chem. Rev. 89 (1989) 1861–1873.
[6] M.A. Shannon, P.W. Bohn, M. Elimelech, J.G. Georgiadis, B.J. Marinas, A.M. Mayes, Nature 452 (2008) 301–310.
[7] Z. Jiang, F. Yang, N. Luo, B.T.T. Chu, D. Sun, H. Shi, T. Xiao, P.P. Edwards, Chem. Commun. (47) (2008) 6372–6374.
[8] F. Han, V.S.R. Kambala, M. Srinivasan, D. Rajarathnam, R. Naidu, Appl. Catal. A 359 (2009) 25–40.
[9] R. Asahi, T. Morikawa, T. Ohwaki, K. Aoki, Y. Taga, Science 293 (2001) 269–271.
[10] S.U.M. Khan, M. Al-Shahry, W.B. Ingler Jr., Science 297 (2002) 2243–2245.
[11] Z. Jiang, F. Al-Shahrani, T.-W. Lin, Y. Cui, T. Xiao, Stud. Surf. Sci. Catal. (2007) 355–359.
[12] X. Shu, Z. An, L. Wang, J. He, Chem. Commun. (39) (2009) 5901–5903.
[13] L. Zhang, W. Wang, L. Zhou, H. Xu, Small 3 (2007) 1618–1625.
[14] Y. Shimodaira, H. Kato, H. Kobayashi, A. Kudo, J. Phys. Chem. B 110 (2006) 17790–17797.
[15] A. Kudo, K. Omori, H. Kato, J. Am. Chem. Soc. 121 (1999) 11459–11467.
[16] S. Tokunaga, H. Kato, A. Kudo, Chem. Mater. 13 (2001) 4624–4628.
[17] H.G. Kim, P.H. Borse, J.S. Jang, E.D. Jeong, O.-S. Jung, Y.J. Suh, J.S. Lee, Chem. Commun. (39) (2009) 5889–5891.
[18] N. Luo, Z. Jiang, H. Shi, F. Cao, T. Xiao, P.P. Edwards, Int. J. Hydrogen Energy 34 (2009) 125–129.
[19] K.-L. Zhang, C.-M. Liu, F.-Q. Huang, C. Zheng, W.-D. Wang, Appl. Catal. B 68 (2006) 125–129.
[20] H. An, Y. Du, T. Wang, C. Wang, W. Hao, J. Zhang, Rare Met. 27 (2008) 243–250.
[21] X. Lin, T. Huang, F. Huang, W. Wang, J. Shi, J. Phys. Chem. B 110 (2006) 24629–24634.
[22] W. Wang, F. Huang, X. Lin, Scripta Mater. 56 (2007) 669–672.
[23] X.-P. Lin, F.-Q. Huang, W.-D. Wang, Z.-C. Shan, J.-L. Shi, Key Eng. Mater. (2008) 368–372;
X.-P. Lin, F.-Q. Huang, W.-D. Wang, Z.-C. Shan, J.-L. Shi, High Perform. Ceram. V (Pt. 2) (2008) 1503–1506.
[24] W. Wang, F. Huang, X. Lin, J. Yang, Catal. Commun. 9 (2008) 8–12.
[25] J. Zhang, F. Shi, J. Lin, D. Chen, J. Gao, Z. Huang, X. Ding, C. Tang, Chem. Mater. 20 (2008) 2937–2941.
[26] X. Zhang, Z. Ai, F. Jia, L. Zhang, J. Phys. Chem. C 112 (2008) 747–753.
[27] M. Shang, W. Wang, L. Zhang, J. Hazard. Mater. 167 (2009) 803–809.
[28] J. Henle, P. Simon, A. Frenzel, S. Scholz, S. Kaskel, Chem. Mater. 19 (2007) 366–373.
[29] A. Rabenau, Angew. Chem. Int. Ed. 24 (1985) 1026–1040.
[30] H. Kodama, S. Horiuchi, A. Watanabe, J. Solid State Chem. 75 (1988) 279–284.
[31] H. Deng, J. Wang, Q. Peng, X. Wang, Y. Li, Chem. Eur. J. 11 (2005) 6519–6524.
[32] J. Wang, Y. Li, Chem. Commun. 18 (2003) 2320–2321.
[33] M.R. Hoffmann, S.T. Martin, W. Choi, D.W. Bahnemann, Chem. Rev. 95 (1995) 69–96.
[34] A.H. Nethercot, Phys. Rev. Lett. 33 (1974) 1088.
[35] M.A. Butler, D.S. Ginley, J. Electrochem. Soc. 125 (1978) 228–232.
[36] H. Fu, C. Pan, W. Yao, Y. Zhu, J. Phys. Chem. B 109 (2005) 22432–22439.
[37] D. Wang, T. Kako, J. Ye, J. Am. Chem. Soc. 130 (2008) 2724–2725.